

Two novel six-coordinated cadmium(II) and zinc(II) complexes from carbazate β -diketonate: crystal structures, enhanced two-photon absorption and biological imaging application†‡

Cite this: *Dalton Trans.*, 2014, **43**, 599

Cuiyun Nie,^{§a} Qiong Zhang,^{§a} Hongjuan Ding,^b Bei Huang,^c Xinyan Wang,^c Xianghua Zhao,^a Shengli Li,^a Hongping Zhou,^a Jieying Wu^{*a} and Yupeng Tian^{*a,d}

To explore the photophysical properties of coordination compounds with enhanced two-photon absorption, two novel six-coordinated metal complexes (ML_2 , $M = Cd(II), Zn(II)$) from carbazole β -diketonate ligand (HL = 4,4,4-trifluoro-1-(9-butylcarbazole-3-yl)-1,3-butanedione) were prepared and fully characterized. Their crystal structures were determined by X-ray diffraction analysis. Both variable temperature 1H NMR spectra and MALDI-TOF mass spectrometry proved that the coordination compounds exhibit good stability in solution. The results of time-dependent density functional theory (TD-DFT) calculations indicated that the complexation of the ligands with metal ion extends the electronic delocalization in the coordination compounds, leading to enhanced two-photon absorption. The photophysical properties for the coordination compounds were identified relying on both experimentally and theoretically studies. Finally, confocal microscopy and two-photon microscopy fluorescent imaging of HepG2 cells labeled with the $Zn(II)$ complex revealed its potential applications as a biological fluorescent probe.

Received 20th May 2013,
Accepted 24th September 2013

DOI: 10.1039/c3dt51318a

www.rsc.org/dalton

Introduction

Two photons are simultaneously absorbed to an excited state in a medium *via* a virtual state, which was first predicted by Göppert-Mayer in 1931.¹ Two-photon absorption (TPA) was possible only 30 years later with the advent of lasers. The first experimental evidence was performed by W. Kaiser and C. G. Garret.² The recent technologies that can exploit TPA materials have received significant applications in the areas of chemistry, biology and photonics, such as optical limiting, two-photon laser scanning fluorescence imaging, micro-fabrication, 3D optical data storage and photodynamic therapy.³ The applications highly rely on the high TPA cross-section of the specifically engineered molecules.⁴ Spurred by this, many

researchers focused to seek novel materials with large TPA cross-section (σ), leading to a great deal of work on building π -conjugated dipolar, quadrupolar, and octupolar molecules with π -centers and functional groups of electron-donating and/or electron-withdrawing groups at the terminal sites.⁵ Their structure–property correlations have been systematically investigated, and molecular design strategies of organic compounds with large σ were well-established.⁶

Apart from the studies of organic compounds for TPA, there has been a growing interest in the study of coordination compounds as TPA materials.⁷ Previously, our group has developed various two-photon materials,⁸ and it is suggested that large TPA cross sections can be brought about by their characteristic intra/inter-ligand and metal-to-ligand charge-transfer transitions during photo-excitation. However, apart from the large TPA values, it is also current challenge that TPA materials should meet various requirements for the specific utility. With the interests and efforts in the design and synthesis of series of coordination compounds,⁸ a program was launched to explore the functional organic ligands to construct novel coordination compounds. Herein, the design, synthesis, characterization, crystal structures, and photophysical properties of two novel coordination compounds based on carbazate β -diketonate ligand were described on the basis of both experiments and theoretical calculation. The ligand (HL), shown in Scheme 1, was designed based on the following

^aDepartment of Chemistry, Key Laboratory of Functional Inorganic Materials Chemistry of Anhui Province, Anhui University, Hefei 230039, P. R. China.

E-mail: jywu1957@163.com, yptian@ahu.edu.cn

^bDepartment of Physics, Shandong Normal University, Jinan 250014, P. R. China

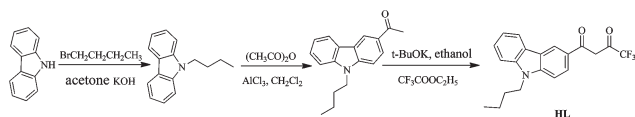
^cDepartment of Biology, Anhui University, Hefei 230039, P. R. China

^dState Key Laboratory of Coordination Chemistry, Nanjing University, Nanjing, 210093, P. R. China

†Dedicated to Professor Xiao-Zeng You for His 80th Birthday.

‡Electronic supplementary information (ESI) available. CCDC 635449 for $Cd(L)_2 \cdot 2H_2O$ and 635450 for $Zn(II)L_2(H_2O)_2$. For ESI and crystallographic data in CIF or other electronic format see DOI: 10.1039/c3dt51318a

§These authors contributed equally to this work.



Scheme 1 Synthesis routes for the preparation of HL.

considerations: (1) carbazole moiety contains conjugated system, bearing good optical properties, carbazole-based materials have potential applications as an electron donor, hole-transport and photoconductive materials, molecular probes and photosensitizer;⁹ (2) β -diketonate unit as a chelate ligand has an interesting coordination chemistry, unusual structural features;¹⁰ (3) $-\text{CF}_3$ group as an electron-withdrawing group to make β -diketonate unit easier to coordinate with metal ion, forming an extended conjugated system; (4) for practical applications, the advantages of the ligand (HL) should be lower molecular weight and easier to be synthesized than those previously reported.^{7,8} The present results proved that the two coordination compounds exhibit significantly enhanced TPA cross-section values compared with those of the free ligand. Furthermore, the connections between the structure and TPA properties were firstly studied depending on both experimentally and theoretically for the novel Zn(II) and Cd(II) complexes, according to our knowledge. Finally, a study of the zinc coordination compound as a biological fluorescent probe was carried out.

Experimental section

Materials and apparatus

All chemicals were commercially available and all solvents were purified by conventional methods before use.

Elemental analyses were performed with a Perkin Elmer 240C elemental analyzer. The ^1H NMR spectra were recorded at 25 °C on a Bruker Avance 400 spectrometer, and the chemical shift are reported as parts per million from TMS (δ). Coupling constants J are given in hertz. Mass spectra were acquired on a Micromass GCT-MS (EI source). IR spectra were recorded on a NEXUS 870 (Nicolet) spectrophotometer in the 400–4000 cm^{-1} region using a powder sample on a KBr plate. XPS spectra were recorded on PHI 5000 Versaprobe spectrophotometer. UV-vis absorption spectra were recorded on a UV-265 spectrophotometer. Fluorescence measurements were carried out on a Hitachi F-7000 fluorescence spectrophotometer. All the fluorescence spectra were collected. The single-photon excited fluorescence (SPEF) quantum yields were measured by using a standard method under the same experimental conditions for all compounds. Two-photon absorption (TPA) cross sections (σ) of the sample were obtained at femtosecond laser pulse and Ti sapphire system (680–1080 nm, 80 MHz, 140 fs) as the light source. All measurements were carried out in air at room temperature. TPA cross-sections were measured using fluorescein as reference.

Measurements

The fluorescence quantum yields (Φ) and fluorescence lifetime (τ). The fluorescence quantum yields (Φ) were determined by using coumarin 307 as the reference according to the literature method.^{10,11} Quantum yields were corrected as follows:

$$\Phi_s = \Phi_r \left(\frac{A_r \eta_s^2 D_s}{A_s \eta_r^2 D_r} \right)$$

where the s and r indices designate the sample and reference samples, respectively, A is the absorbance at λ_{exc} , η is the average refractive index of the appropriate solution, and D is the integrated area under the corrected emission spectrum.¹²

Fluorescence lifetime is traditionally considered to be a kinetic parameter and is determined as being inversely proportional to the sum rate constants of a radiative process k_r and the nonradiative processes k_{nr} collectively known as quenching.

$$\tau = 1/(k_r + \sum k_i)$$

$$\Phi = k_r/(k_r + k_{\text{nr}})$$

where $\sum k_i$ is the sum of the rate constant of non-radiative transition process, k_r is the rate constant of a radiative process and k_{nr} is the cumulative rate constant of a nonradiative processes.

TPA cross-section (σ). TPEF (two photon excited fluorescence) spectra were measured using femtosecond laser pulse and Ti:sapphire system (680–1080 nm, 80 MHz, 140 fs, Chameleon II) as the light source. All measurements were carried out in air at room temperature. TPA cross sections were measured using two-photon-induced fluorescence measurement technique. The TPA cross sections (σ) are determined by comparing their TPEF to that of fluorescein in different solvents, according to the following equation:¹³

$$\sigma = \sigma_{\text{ref}} \frac{\Phi_{\text{ref}} c_{\text{ref}} n_{\text{ref}} F}{\Phi c n F_{\text{ref}}}$$

Here, the subscripts ref stands for the reference molecule. σ_{ref} is the TPA cross-section value, c is the concentration of solution, n is the refractive index of the solution, F is the TPEF integral intensities of the solution emitted at the exciting wavelength, and Φ is the fluorescence quantum yield. The σ_{ref} value of reference was taken from the literature.¹⁴

Fluorescence lifetime

For time-resolved fluorescence measurements, the fluorescence signals were collimated and focused onto the entrance slit of a monochromator with the output plane equipped with a photomultiplier tube (HORIBA HuoroMax-4P). The decays were analyzed by 'least-squares'. The quality of the exponential fits was evaluated by the goodness of fit (χ^2).

The Stokes shift

The Stokes shift is defined as the loss of energy between absorption and emission of light, which is a result of several

dynamic processes. These processes include losses arising from the dissipation of vibrational energy, redistribution of electrons in the surrounding solvent molecules induced by the altered dipole moment of the excited compound, reorientation of the solvent molecules around the excited state dipole, and specific interactions between the compound and the solvent or solutes. The Lippert equation is the most widely used equation to describe the effects of the physical properties of the solvent on the emission spectra of a compound.¹⁵

$$\Delta\nu = \nu_{\text{abs}} - \nu_{\text{em}} = (2/eha^3)\Delta f(\mu_e - \mu_g)^2 + \text{const}$$

In this equation, h is Planck's constant, e is the speed of light, and a is the radius of the cavity in which the compound resides. The wave numbers of the absorption and emission are ν_{abs} and ν_{em} (in cm^{-1}).

Cell image

HepG2 cells were seeded in 6 well plates at a density of 2×10^5 cells per well and grown for 96 hours. For live cell imaging cell cultures were incubated with the complexes (10% PBS:90% cell media) at concentrations 20 μM and maintained at 37 °C in an atmosphere of 5% CO_2 and 95% air for incubation times ranging for 2 hours. The cells were then washed with PBS (3 \times 3 mL per well) and 3 mL of PBS was added to each well. The cells were imaged using confocal laser scanning microscopy and water immersion lenses. Excitation energy of 720 nm was used and the fluorescence emission measured at 461–511 nm.

Microscopy

HepG2 cells were imaged on a Zeiss LSM 710 META upright confocal laser scanning microscope using magnification 40 \times and 100 \times water-dipping lenses for monolayer cultures. Image data acquisition and processing was performed using Zeiss LSM Image Browser, Zeiss LSM Image Expert and Image J.

Cytotoxicity assays in cells

To ascertain the cytotoxic effect of all the compounds treatment over a 24 h period, the 5-dimethylthiazol-2-yl-2,5-diphenyltetrazolium bromide (MTT) assay was performed. HepG2 cells were trypsinized and plated to ~70% confluence in 96-well plates 24 h before treatment. Prior to the compounds' treatment, the DMEM was removed and replaced with fresh DMEM, and aliquots of the compound stock solutions (500 μM DMSO) were added to obtain final concentrations of 20, 40, 60, 80 and 100 μM . The treated cells were incubated for 24 h at 37 °C and under 5% CO_2 . Subsequently, the cells were treated with 5 mg mL^{-1} MTT (40 μL per well) and incubated for an additional 4 h (37 °C, 5% CO_2). Then, DMEM was removed, the formazan crystals were dissolved in DMSO (150 μL per well), and the absorbance at 490 nm was recorded. The cell viability (%) was calculated according to the following equation: cell viability % = $\text{OD}_{490}(\text{sample})/\text{OD}_{490}(\text{control}) \times 100$, where $\text{OD}_{490}(\text{sample})$ represents the optical density of the

wells treated with various concentration of the compounds and $\text{OD}_{490}(\text{control})$ represents that of the wells treated with DMEM + 10% FCS. Three independent trials were conducted, and the averages and standard deviations are reported. The reported percent cell survival values are relative to untreated control cells.

Density functional theory (DFT) calculation

The two-photon absorption cross-section that can be directly compared with the experimental results is defined as:

$$\sigma_{\text{tp}} = \frac{4\pi^2 a_0^5 \alpha}{15e_0} \times \frac{\omega^2 g(\omega)}{\Gamma_f} \delta_{\text{tp}}$$

Here a_0 is the Bohr radius, e_0 is the speed of light, α is the fine structure constant, ω is the photon frequency of the incident light, and $g(\omega)$ denotes the spectral line profile, which is assumed to be a δ function here, Γ_f is the lifetime broadening of the final state, which is commonly assumed to be 0.1 eV,¹⁶ and δ_{tp} is orientation average value of the two-photon absorption probability in gas and solution, which is written as follows,¹⁷

$$\delta_{\text{tp}} = \sum_{\alpha\beta} [F \times S_{\alpha\alpha} \times S_{\beta\beta}^* + G \times S_{\alpha\beta} \times S_{\alpha\beta}^* + H \times S_{\alpha\beta} \times S_{\beta\alpha}^*]$$

where F , G , and H are coefficients dependent on the polarization of the light. For the linearly polarized light, F , G and H are 2, 2, 2, for the circularly case, they are -2 , 3, 3. $S_{\alpha\beta}$ is the two-photon transition matrix element. For the absorption of two photons with the same frequency $\omega_f/2$ it can be written as,¹⁸

$$S_{\alpha\beta} = \sum_i \left[\frac{\langle 0|\mu_\alpha|i\rangle\langle i|\mu_\beta|f\rangle}{\omega_i - \omega_f/2} + \frac{\langle 0|\mu_\beta|i\rangle\langle i|\mu_\alpha|f\rangle}{\omega_i - \omega_f/2} \right]$$

where ω_i and ω_f denote the excitation frequency of the intermediate state $|i\rangle$ and final state $|f\rangle$ respectively, $\alpha, \beta \in (x, y, z)$, and the summation goes over all the intermediate states including the ground state $|0\rangle$ and the final state $|f\rangle$.

Optimizations were carried out with B3LYP[LAN2DZ] without any symmetry restraints, and the TD-DFT {B3LYP-[LAN2DZ]} calculations were performed on the optimized structure.^{19a} All calculations, including optimizations and TD-DFT, were performed with the G03 software.^{19b} Geometry optimization of the singlet ground state and the TDDFT calculation of the lowest 25 singlet-singlet excitation energies were calculated with a basis set composed of 6-31G(d,p) for C, N, H, F, O atoms and the Lan12dz basis set for Zn and Cd atom was downloaded from the EMSL basis set library. An analytical frequency analysis provides evidence that the calculated species represents a true minimum without imaginary frequencies on the respective potential energy surface. In the calculation of the absorption spectrum, the 25 lowest spin-allowed singlet-singlet transitions, up to energy of about 5 eV, were taken into account (Table S3†) The calculation two-photon absorption is carried out by the response theory method²⁰ at the DFT level implemented in DALTON program.²¹

Synthesis

HL (Scheme 1) was synthesized by a modified method of typical Claisen condensation procedure.²²

9-Butyl-carbazole. To a solution of 9-H-carbazole (16.7 g, 100 mmol) and KOH (8.4 g, 150 mmol) in acetone (100 mL) was refluxed for 2 hours. After cooling to room temperature, 14 mL 1-bromination butane (13.7 g, 100 mmol) were added and refluxed for 24 hours. 200 mL water was added with stirring after removing the solvent. The residual solid was recrystallized from ethanol to give colorless crystals (18.4 g, yield 83%). Ms *m/z* (%): 223.14(100). Anal. Calc. for C₁₆H₁₇N: C 86.05, H 7.67, N 6.27%; found C 86.02, H 7.65, N 6.23%.

3-Acetyl-9-butyl-carbazole. To a solution of 9-butyl-carbazole (4.4 g, 20 mmol) in dichloromethane (70 mL) was rapidly added AlCl₃ (5.2 g, 40 mmol) with stirring. After cooling to 0 °C, a solution of acetic anhydride (2.04 g, 20 mmol) in 20 mL of dichloromethane was added dropwise under stirring. After stirring over night at room temperature, a large amount of water and HCl were added into the mixture and extracted with dichloromethane twice, washed by 1 M NaHCO₃ and water. The combined organic phase was dried over anhydrous MgSO₄ and then filtered. The organic solvent was completely removed by rotary evaporation. The solid was purified by column chromatograph (silica gel, ethyl acetate–petroleum ether = 1:4 as eluent) to give the purified title compound (4.0 g, 76%). Ms *m/z* (%): 265.13(100). Anal. Calc. for C₁₈H₁₉NO: C 81.47, H 7.22, N 5.28; found C 81.41, H 7.25, N 5.26.

4,4,4-Trifluoro-1-(9-butylcarbazole-3-yl)-1,3-butanedione (HL). To a solution of ethyl trifluoroacetate (1.71 g, 12 mmol) in anhydrous ethanol (20 mL) was added *t*-BuOK (3.33 g, 15 mmol). A solution of 3-acetyl-9-butyl-carbazole (2.64 g, 10 mmol) in 10 mL of anhydrous ethanol was added dropwise, and then stirring for 5 hours at room temperature. After 3 M HCl was added to the mixture with stirring, the mixture was extracted with dichloromethane and the organic layer was collected. The organic layer was dried over anhydrous MgSO₄ and filtered. The organic solvent was completely removed by rotary evaporation. The residue was purified by recrystallized from the petroleum ether and ethyl acetate to give the yellowish crystals of the title compound (3.05 g, 85%). MS *m/z* (%): 361.02 (100). ¹H NMR (400 MHz, DMSO-*d*₆) δ 14.23 (s, 1H), 9.13 (s, 1H), 8.34 (d, *J* = 7.6 Hz, 1H), 8.23 (d, *J* = 8.8 Hz, 1H), 7.77 (d, *J* = 8.80 Hz, 1H), 7.71 (d, *J* = 8.0, 1H), 7.55 (t, *J* = 7.6 Hz, 1H), 7.33 (t, *J* = 7.4, 1H), 7.21 (s, 1H), 4.46 (s, 1H), 1.76 (t, *J* = 7.0, 2H), 1.30 (d, *J* = 7.2, 2H), 0.87 (t, *J* = 7.2, 3H). IR (KBr pellet, cm⁻¹): 3414 (m), 2988 (w), 2966 (w), 1272 (s), 1599 (vs), 1496 (m), 1474 (m), 792 (m), 578 (w).

Cd(II)L₂(H₂O)₂. To an aqueous of Cd(NO₃)₂·4H₂O (0.3085 g, 1 mmol) 3 mL was added dropwise to a solution of HL (0.7220 g, 2 mmol) in ethanol (15 mL) neutralized with 2 mL triethylamine. Then, the mixture was stirred at 80 °C for 12 hours. The precipitated product was filtered and washed by ethanol and tetrahydrofuran. The product was dried at 80 °C in vacuum for 12 hours. Yield: 0.70 g (80%). ¹H NMR

(400 MHz, DMSO-*d*₆): 8.27 (s, 1H), 8.13 (d, 1H), 7.65 (d, *J* = 10.0 Hz, 1H), 7.55–7.44 (m, 3H), 7.31 (d, *J* = 4.0 Hz, 1H), 6.84 (s, 1H), 4.35 (m, 2H), 3.76–3.70 (m, 2H), 1.44–1.37 (m, 2H), 1.26–1.22 (m, 2H), 0.96 (t, *J* = 6.8 Hz, 3H). IR (KBr pellet, cm⁻¹): 3415 (m), 2956 (w), 2871 (w), 1269 (s), 1616 (vs), 1494 (m), 1469 (m), 789 (m), 580 (w).

Zn(II)L₂(H₂O)₂. An aqueous of Zn(NO₃)₂·6H₂O (0.37g, 1 mmol) 3 mL was added dropwise to a solution of HL (0.72 g, 2 mmol) in ethanol and tetrahydrofuran (15 mL, ethanol–tetrahydrofuran = 5:1), which had been neutralized with 2 mL triethylamine. Then, the mixture was stirred at 80 °C for 12 hours. The precipitated product was filtered and washed by ethanol and tetrahydrofuran. The product was dried at 80 °C in vacuum for 12 hours. Yield: 0.66 g (80%). ¹H NMR (400 MHz, DMSO-*d*₆): 8.76 (s, 1H), 8.38 (s, 1H), 8.04 (d, *J* = 8.7 Hz, 1H), 7.60 (d, *J* = 8.19 Hz, 2H), 7.45 (t, *J* = 7.6 Hz, 1H), 7.16 (s, 1H), 6.46 (s, 1H), 4.38 (t, *J* = 6.5 Hz, 2H), 3.59–3.56 (m, 2H), 1.27–1.21 (m, 2H), 0.81 (t, *J* = 7.3 Hz, 3H).

X-ray crystallography

Intensity data of 1 was collected with Mo-K_α radiation ($\lambda = 0.71073 \text{ \AA}$) on a Bruker SMART Apex CCD diffractometer at 293 K. Absorption corrections were applied by using SADABS.²³ The structures were solved by WinGX package²⁴ and refined by full-matrix least-squares with anisotropic thermal parameters for all the nonhydrogen atoms using SHELXL-97.²⁵ Hydrogens were included and located from difference Fourier map but not refined anisotropically. Crystal data collections and refinement parameters of Cd(II)L₂(H₂O)₂ and Zn(II)-L₂(H₂O)₂ are shown in Table S1.‡ Selected bond lengths and angles for Cd(II)L₂(H₂O)₂ and Zn(II)L₂(H₂O)₂ are listed in Table S2.‡

Results and discussion

Characterizations of the coordination compounds

The pH value in the reaction solution is an important factor for the complexation formation of M(II)L₂(H₂O)₂, in which the pH value was adjusted to 7.0 with triethylamine. The IR spectra of M(II)L₂(H₂O)₂ show features attributed to each part of them, in which the coordinated water molecules cause a stronger band at 3415 cm⁻¹ than that of the ligand. Herein, we take Cd(II)L₂(H₂O)₂ as an example to assign the bands. The bands of 2956 cm⁻¹ and 789 cm⁻¹ are assigned to $\nu_{\text{C-H}}$ of carbazole ring. In addition, the bands at 1494 and 1469 cm⁻¹ are attributed to the stretching vibration of the carbazole ring. Then the band located at 1616 cm⁻¹ is attributed to the stretching vibration of carbonyl, which has a blue shift because of the coordination with metal ion. The shape and location of the other bands are consistent with those of the ligand.

To further prove the stability of the coordination compounds, the variable temperature ¹H NMR spectra of Zn(II)-L₂(H₂O)₂, as an example, shown in Fig. S1.‡ MALDI-TOF mass spectrometry was used to further verify the stability of

$\text{Zn(II)L}_2(\text{H}_2\text{O})_2$ in DMSO solution. The results suggest that the coordination compounds are very stable in DMSO solution, which belongs to the molecular weight of the structure $\text{Zn(II)-L}_2(\text{H}_2\text{O})_2$ (more detailed information is shown in Fig. S2 \ddagger), that shows that the two coordinated water molecules in the complex do not decompose in solution. The results of spectral characterization are consistent with those of single crystal X-ray diffraction analysis as below.

Crystal structures of $\text{Cd(II)L}_2(\text{H}_2\text{O})_2$ and $\text{Zn(II)L}_2(\text{H}_2\text{O})_2$

$\text{Cd(II)L}_2(\text{H}_2\text{O})_2$ crystallizes in the monoclinic space group $C2/c$, as shown in Fig. 1. Cd(II) ion has distorted octahedral geometry with four oxygen atoms from two HL in the equatorial positions and two oxygen atoms from two water molecules at the axial positions. The bond lengths²⁶ of Cd(1)-O(3) , Cd(1)-O(5) , Cd(1)-O(6) are 2.361(3), 2.227(3) and 2.230(3) Å, respectively. Each bond angle around the cadmium atom is in the range 83.37(11)–96.63(11)°, indicating a distorted octahedral geometry.

$\text{Zn(II)L}_2(\text{H}_2\text{O})_2$ also crystallizes in the monoclinic space group $C2/c$, as shown in Fig. 2. Similar to $\text{Cd(II)L}_2(\text{H}_2\text{O})_2$, Zn(II) ion center in the coordination compound $\text{Zn(II)L}_2(\text{H}_2\text{O})_2$ also adopts a slightly distorted octahedral geometry with four oxygen atoms from HL on the equatorial plane, two oxygen donors from two water molecules at the apical positions. The bond lengths Zn(1)-O(1) , Zn(1)-O(2) , Zn(1)-O(3) are 2.053(5), 2.033(5) and 2.239(5) Å, respectively. Each bond angle around the zinc atom is in the range 89.4(2)–90.6(2)°.

As shown in Table S2, \ddagger the bond length of Cd-O is longer than that of Zn-O . In addition, the radius of Cd atom is larger,

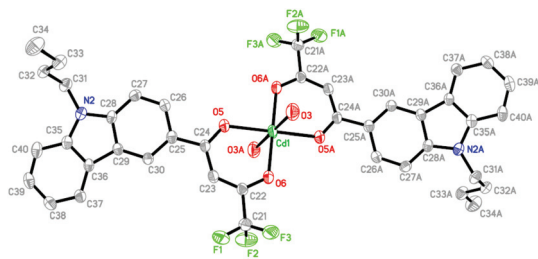


Fig. 1 Coordination environments of $\text{Cd(II)L}_2(\text{H}_2\text{O})_2$ with the atom numbering scheme.

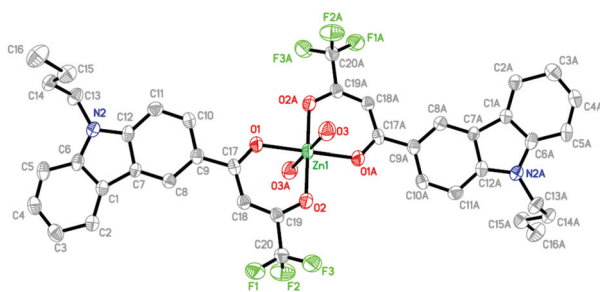


Fig. 2 Coordination environments of $\text{Zn(II)L}_2(\text{H}_2\text{O})_2$ with the atom numbering scheme.

so $\text{Cd(II)L}_2(\text{H}_2\text{O})_2$ has a larger conjugate plane. From the bond lengths of M-O we can see that $\text{Cd(II)L}_2(\text{H}_2\text{O})_2$ is in a more distorted octahedral geometry.

The carbonyl bond lengths of $\text{Cd(II)L}_2(\text{H}_2\text{O})_2$ for C22-O6 and C24-O5 are 1.279 and 1.257 Å, respectively. The carbonyl bond lengths of $\text{Zn(II)L}_2(\text{H}_2\text{O})_2$ for C19-O2 and C17-O1 are 1.282 and 1.256 Å, respectively. Interestingly, the two coordinated ligands are almost co-planar (4.70° for $\text{Zn(II)-L}_2(\text{H}_2\text{O})_2$ and 8.10° for $\text{Cd(II)L}_2(\text{H}_2\text{O})_2$) in the coordination compounds. Therefore, it was observed that the bond lengths of C-O of the diketone become longer than those of the free ligand after coordinating to metal ions Cd(II) , Zn(II) , resulting in an extending conjugated system.^{8b} The structural features reveal that the two compounds will possess a good optical properties.

UV-vis spectra and TD-DFT studies

The UV absorption spectra of HL, $\text{Cd(II)L}_2(\text{H}_2\text{O})_2$ and $\text{Zn(II)-L}_2(\text{H}_2\text{O})_2$ (1.0×10^{-6} M in THF) are shown in Fig. 3. As can be seen, HL exhibits an absorption band at 349 nm with the corresponding molar extinction coefficient ($\epsilon = 5.11 \times 10^4 \text{ M}^{-1} \text{ cm}^{-1}$), which was assigned as the intramolecular charge transfer (ICT) transition [$\pi_{\text{carbazole}} \rightarrow \pi^*_{\text{COCHC(OH)CF}_3}$] due to the $\text{H} \rightarrow \text{L}$ transition.^{8b} The both compounds, $\text{Cd(II)L}_2(\text{H}_2\text{O})_2$ and $\text{Zn(II)-L}_2(\text{H}_2\text{O})_2$, exhibit an absorption band around 278 nm with the corresponding molar extinction coefficient ($\epsilon = 6.21 \times 10^4 \text{ M}^{-1} \text{ cm}^{-1}$ for $\text{Cd(II)L}_2(\text{H}_2\text{O})_2$ and $6.50 \times 10^4 \text{ M}^{-1} \text{ cm}^{-1}$ for $\text{Zn(II)-L}_2(\text{H}_2\text{O})_2$), which originates from the $\text{n} \rightarrow \pi^*$ transition of the carbazole unit. Besides, the both UV-visible spectra of $\text{Cd(II)-L}_2(\text{H}_2\text{O})_2$ and $\text{Zn(II)L}_2(\text{H}_2\text{O})_2$ exhibit one characteristic absorption band at λ_{max} 339 and 334 nm assigned to M-L(L)CT ((Cd , Zn center)-to-carbazole excitation).²⁷

By comparing the UV-vis absorption spectra of $\text{Zn(II)-L}_2(\text{H}_2\text{O})_2$, $\text{Cd(II)L}_2(\text{H}_2\text{O})_2$ and HL in the same concentration, it was found that the extinction coefficients of $\text{Zn(II)L}_2(\text{H}_2\text{O})_2$ and $\text{Cd(II)L}_2(\text{H}_2\text{O})_2$ are 2-fold less than that of HL in solution. It can be explained that the spectra observed should arise from the whole complex molecules rather than the dissociated molecules in the solution (Fig. S1 and S2 \ddagger). The stability of the coordination compounds was verified by the results of the variable temperature ^1H NMR spectra and MALDI-TOF mass spectrometry. It should be noted that the structural changes have

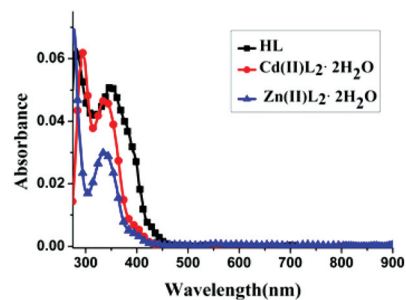


Fig. 3 UV-vis absorption spectra of HL, $\text{Cd(II)L}_2(\text{H}_2\text{O})_2$ and $\text{Zn(II)L}_2(\text{H}_2\text{O})_2$ (1.0×10^{-6} M in THF).

taken place when the complexation formation of $M(II)L_2(H_2O)_2$ after deprotonation of the free ligands.

TD-DFT computational studies were performed to elucidate the electronic structures of the ground state of $Cd(II)L_2(H_2O)_2$ and $Zn(II)L_2(H_2O)_2$. The molecular orbital diagrams of HL, $Cd(II)L_2(H_2O)_2$ and $Zn(II)L_2(H_2O)_2$ were shown in Fig. 4, respectively. The energies and compositions of some frontier orbitals are listed in Table S3.†

As shown in Fig. 4 and Fig. S5,† the HOMOs (H) and H-1 of HL are of π orbitals localized on the carbazole and COCHC(OH)CF₃ groups. The unoccupied molecular orbitals LUMO (L) and L+1 are of the carbazole and COCHC(OH)C₆H₅ units. The HOMO and H-1 of $Zn(II)L_2(H_2O)_2$ are of the π orbitals on COCHC(OH)CF₃ and Zn center. LUMO and L+1 are of π^* orbitals localized on the whole molecule. As shown in Table S3,† the lowest-energy excitation bands of the two complexes ($\lambda = 353.91$ nm and $f = 0.0011$ for $Cd(II)L_2(H_2O)_2$, $\lambda = 351.00$ nm and $f = 0.0021$ for $Zn(II)L_2(H_2O)_2$) are assigned as the MLCT mixed with $\pi_{(C(OH)COCF_3)} \rightarrow \pi^*_{(COCHC(OH)C_6H_5)}$ transition due to the H-1 \rightarrow L transition, whereas those of the transitions at 277.16 nm for $Cd(II)L_2(H_2O)_2$ and 283.63 nm for $Zn(II)L_2(H_2O)_2$ in the high-energy absorption regions are mainly due to the

H-1 \rightarrow L+2 and H \rightarrow L+3 transition [$n \rightarrow \pi^*_{(COCHC(OH)C_6H_5)}$]. It is inferred that the oscillator strengths of the high-energy absorption bands of both ligands are larger than those of the low-energy bands. Basically, the calculated singlet-singlet transitions in $Cd(II)L_2(H_2O)_2$ and $Zn(II)L_2(H_2O)_2$ are in reasonable agreement with the extended electron delocalization drawn from the crystal structure determination. Finally, XPS (Fig. S3†) determination results also show the atomic concentration sequence of the coordination site O atom is $Cd(II)L_2(H_2O)_2$ (16.89) > $Zn(II)L_2(H_2O)_2$ (13.78) > HL (12.12), which was in accordance with the electron delocalization tendency calculated.

Single-photon excited fluorescence (SPEF)

The SPEF spectra were measured at the same concentration as that of the linear absorption spectra. Surprisingly, the SPEF spectra of HL, $Cd(II)L_2(H_2O)_2$ and $Zn(II)L_2(H_2O)_2$ display pronounced negative solvatochromism blue shift with increasing polarity of the solvents (Table 1). This can be explained by the fact that the ground state may possess a higher polarity than the excited state, for negative solvatochromism is associated with a increasing of the energy levels. A decreased dipole-

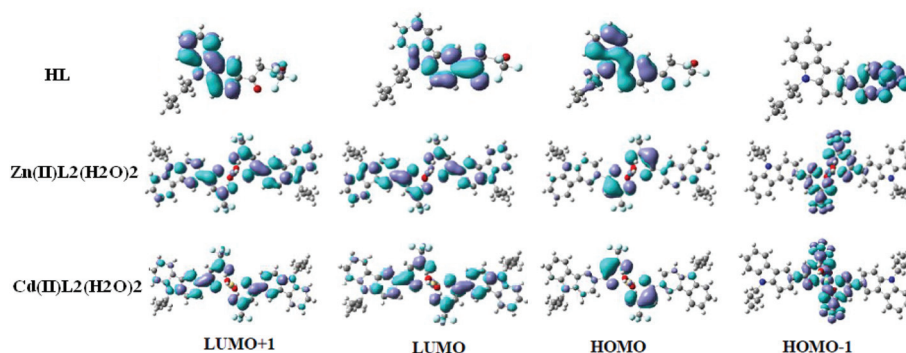


Fig. 4 Molecular orbital diagram for HL (B3LYP/6-31G(d)), $Zn(II)L_2(H_2O)_2$ (B3LYP/LANL2DZ) and $Cd(II)L_2(H_2O)_2$ (B3LYP/LANL2DZ) (the two colors of electron clouds is representative of the square of the wave function of atomic orbitals).

Table 1 Single-photon-related photophysical properties of HL, $Cd(II)L_2(H_2O)_2$ and $Zn(II)L_2(H_2O)_2$ in several different solvents

Compound	Solvents	λ_{max}^a	λ_{max}^b	ϵ	Φ^c	$\Delta\nu^d$ (cm ⁻¹)	T (ns)	$K_f(10^9)$	$K_{nr}(10^9)$
HL	CH ₂ Cl ₂	357	477	23 301	0.23	4161	0.24	1.21	2.96
	THF	349	461	51 089	0.24	3561	0.22	2.50	2.05
	CH ₃ COOC ₂ H ₅	394	460	23 786	0.29	3642	0.20	1.75	3.25
	CH ₃ CH ₂ OH	362	459	29 845	0.46	3339	0.23	2.85	2.15
	DMF	364	450	19 800	0.37	7898	0.80	0.79	0.46
$Cd(II)L_2(H_2O)_2$	CH ₂ Cl ₂	330	475	26 529	0.29	5685	3.65	0.06	0.21
	THF	339	462	48 000	0.55	5677	1.52	0.16	0.50
	CH ₃ COOC ₂ H ₅	364	458	56 798	0.35	5638	0.26	1.11	2.73
	CH ₃ CH ₂ OH	345	461	47 700	0.57	5932	0.75	0.61	0.72
	DMF	345	442	47 000	0.63	7137	0.15	2.47	2.47
$Zn(II)L_2(H_2O)_2$	CH ₂ Cl ₂	339	479	42 500	0.39	5719	3.67	0.11	0.17
	THF	334	468	31 800	0.76	5945	1.97	0.39	0.12
	CH ₃ COOC ₂ H ₅	366	462	35 237	0.36	5955	2.80	0.13	0.22
	CH ₃ CH ₂ OH	354	467	41 900	0.61	6520	2.10	0.31	0.20
	DMF	339	455	68 200	0.74	7092	0.73	1.01	0.36

^a Peak position of the largest absorption band. ^b Peak position of SPEF, excited at the absorption maximum. ^c Quantum yields determined by using RhB as standard. ^d Stokes' shift in cm⁻¹. The experimental errors are estimated to be $\pm 10\%$ from sample concentrations and instruments.

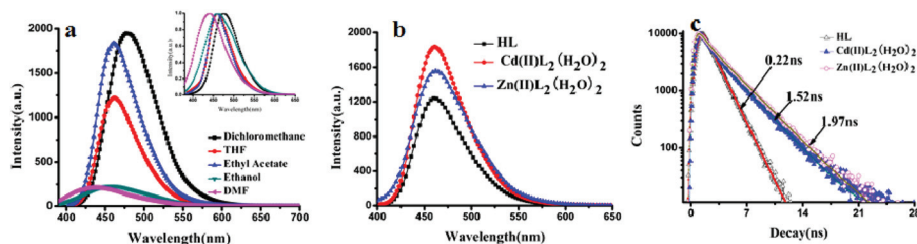


Fig. 5 (a) The one-photon fluorescence spectra of Cd(II)L₂(H₂O)₂ in different solvents. (b) The one-photon fluorescence spectra of HL (1.0×10^{-6} M in ethyl acetate). (c) The time resolved fluorescence curves of HL ($\lambda_{\text{ex}} = 340$ nm, $\lambda_{\text{em}} = 461$ nm), Cd(II)L₂(H₂O)₂ ($\lambda_{\text{ex}} = 340$ nm, $\lambda_{\text{em}} = 462$ nm) and Zn(II)L₂(H₂O)₂ ($\lambda_{\text{ex}} = 340$ nm, $\lambda_{\text{em}} = 468$ nm) (1.0×10^{-5} M in THF).

dipole interaction between the solute and solvent molecules leads to an increasing the energy level.^{8c,e}

As shown in Fig. 5a, the emission maximal of Cd(II)-L₂(H₂O)₂ is about 475 nm in CH₂Cl₂. In high polar solvent DMF, the band is located at 442 nm, which is blue-shifted by 33 nm due to the different molecular environment. Such behaviour is consistent with a symmetry breaking in the ground state. When D–A structural molecule is in a high polar solvent, the molecule in the ground state tends to be polarized to form a charge-separated molecule by the action of an electric field formed by the surrounding solvent molecules. Large Stokes shift (Table 1) is observed for HL, Cd(II)L₂(H₂O)₂ and Zn(II)-L₂(H₂O)₂ in the five solvents due to the strong solvent–solute dipole–dipole interactions, a manifestation of the large dipole moment and orientation polarizability. And the fluorescent quantum yield decrease along with the increasing polarity of the solvents is consistent with the blue-shift of their spectra.^{7c} From Fig. 5b shown that the one-photon fluorescence intensity of the coordination compounds (Cd(II)L₂(H₂O)₂, Zn(II)L₂(H₂O)₂) is stronger than that of the ligand because of the formation of the higher electron delocalization in the coordination compounds.

The enhanced fluorescence also showed corresponding significant changes in emission lifetime, as illustrated by the time resolved fluorescence curves in Fig. 5(c) in THF (0.22, 1.52, 1.97 ns for HL, Cd(II)L₂(H₂O)₂ and Zn(II)L₂(H₂O)₂, respectively). The fluorescence lifetime is the time required by a population of excited fluorophores to decrease exponentially to N/e via the loss of energy through fluorescence and other non-radiative processes.²⁸ Since this process is affiliated with an energetically unstable state, fluorescence lifetime can be sensitive to a great variety of internal factors defined by the fluorophore structure and external factors including temperature and polarity. The coordination compounds (Cd(II)L₂(H₂O)₂, Zn(II)L₂(H₂O)₂) contain more electron-donating group (carbazole) and an electron-withdrawing group (–CF₃). Consequently, it can be seen that a larger conjugated plane and higher polarity result in the longer lifetime than that of the free ligand.

As seen in Table 1, the fluorescence spectra showed moderate Stokes shifts depending on the solvent polarity. Further, the solvatochromism is observed, suggesting a large change in dipole moment between ground and excited states. The Lippert–Mataga equation is the most widely used to

evaluate the dipole moment changes of the dyes with photoexcitation:^{29,30}

$$\Delta\nu = \frac{2\Delta f}{4\pi\epsilon_0 h c a^3} (\mu_e - \mu_g)^2 + b \quad (1)$$

$$\Delta f = \frac{\epsilon - 1}{2\epsilon + 1} - \frac{n^2 - 1}{2n^2 + 1} \quad (2)$$

in which $\Delta\nu = \nu_{\text{abs}} - \nu_{\text{em}}$ stands for Stokes shift, ν_{abs} and ν_{em} are absorption and emission (cm^{-1}), h is the Planck's constant, c is the velocity of light in vacuum, a is the Onsager radius and b is a constant. Δf is the orientation polarizability, μ_e and μ_g are the dipole moments of the emissive and ground states, respectively and ϵ_0 is the permittivity of the vacuum. $(\mu_e - \mu_g)^2$ is proportional to the slope of the Lippert–Mataga plot.

Plots of the Stokes shifts as a function of the solvent polarity factor Δf are shown in Fig. 6. Only the data involving the aprotic solvents are shown because application of this analysis with solvents where specific solute–solvent interactions are present is not appropriate. As shown in Fig. 6, the Lippert–Mataga plot of HL gave much larger slope than Cd(II)L₂(H₂O)₂ and Zn(II)L₂(H₂O)₂, which infers larger dipole moment changes for two complexes with photoexcitation. The slope of the best-fit line is related to the dipole moment change between the ground and excited states ($\mu_e - \mu_g$). The slopes of all three lines are different: 4776, 3581 and 2748 cm^{-1} for HL, Cd(II)L₂(H₂O)₂ and Zn(II)L₂(H₂O)₂, respectively. So the values of $\mu_e - \mu_g$ were calculated as 8.49 D for HL, 11.75 D for Cd(II)-

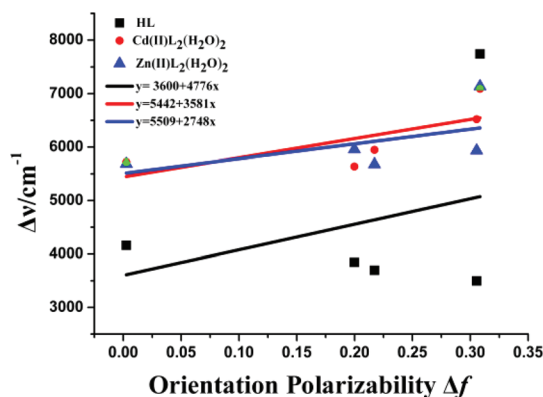


Fig. 6 Lippert–Mataga regressions of the three compounds.

$L_2(H_2O)_2$ and 9.87 D for $Zn(II)L_2(H_2O)_2$, respectively (eqn (1)). The values of $Cd(II)L_2(H_2O)_2$ and $Zn(II)L_2(H_2O)_2$ indicates that the molecule in the excited state has an extremely polar structure,³¹ an enhanced TPA response found in the complexes comparing with HL may be caused by that the equatorial coordination sphere is more coplanar in $Cd(II)L_2(H_2O)_2$ and $Zn(II)L_2(H_2O)_2$ than that in HL, leading to a higher degree of π -electron delocalization, which is proved by the crystal structures and in good agreement with their nonlinear optical properties as shown in Fig. 8.

Two-photon excited fluorescence (TPEF)

As shown in UV-vis spectra of the compounds (Fig. 3), there is no linear absorption in the wavelength range 680–900 nm for them, indicating that there are no energy levels corresponding to an electron transition in this spectral range. Fig. 7a (inset figure) shows a log-log plot of the excited fluorescence signal *versus* excited light power. It provides direct evidence for the squared dependence of excited fluorescence power and input laser intensity upon excitation with a tunable laser in this range, therefore, it should be safely assigned to two-photon excited fluorescence (TPEF). As shown in Fig. 7a, the TPA spectra of HL, $Cd(II)L_2(H_2O)_2$ and $Zn(II)L_2(H_2O)_2$ are determined in the wavelength range by investigating their two-photon excited fluorescence (TPEF) in ethyl acetate with a concentration of 1.0×10^{-3} mol L^{-1} at 720 nm. It can be seen clearly that all the two-photon excited fluorescence (TPEF) spectra of the compounds exhibited a broad emission band,

and the bands show a red shift, compared to the SPEF spectra of them. Furthermore, from the figure, large difference observed between the coordination compounds and its free ligand, which may arise from their different electronic structure, as a result of the ligands bonded to the metal ion to form an extended π -conjugated system in the coordination compound molecules after deprotonation, which were consistent with the results of structural determination above.

It has been found that the two-photon absorption cross sections of coordination compounds ($Cd(II)L_2(H_2O)_2$, $Zn(II)L_2(H_2O)_2$) are remarkably enhanced compared with that of HL in the determined wavelength range (Fig. 7b). The behaviour observed here in the TPA spectra can be attributed to the extending conjugation after complexation of the ligand with $Cd(II)$ or $Zn(II)$ ions, in which the ICT states also play an important role for TPA sections of the coordination compounds. The increased TPA values were observed from $Zn(II)$ to $Cd(II)$ ion possibly gives an extended delocalization. As shown in Table 2, the experimental results are nearly in accordance with those from DFT calculations. The largest two-photon absorption cross-sections of the molecules are 277.25 for $Cd(II)L_2(H_2O)_2$, 179.40 for $Zn(II)L_2(H_2O)_2$ and 11.94 for HL, respectively, which is also consistent with experimental trend ($\sigma(Cd(II)L_2(H_2O)_2) > \sigma(Zn(II)L_2(H_2O)_2) > HL$). This large TPA response comes from the marked core to periphery charge redistribution in $Cd(II)L_2(H_2O)_2$ and $Zn(II)L_2(H_2O)_2$ upon photoexcitation. Therefore, complexation with $Zn(II)$ and $Cd(II)$ enhances the electron-acceptor character of the central β -diketonate group, which converts the ligand to a more strongly polarized D- π -A unit, making the complexes a potential candidate for TPA responses. Moreover, the variation tendency of fluorescence intensity ($Cd(II)L_2(H_2O)_2 > Zn(II)L_2(H_2O)_2 > HL$) is consistent with the results of the fluorescence lifetime ($Cd(II)L_2(H_2O)_2 > Zn(II)L_2(H_2O)_2 > HL$) because the ligand coordinates with the ion M^{2+} ($M = Cd(II), Zn(II)$). At present condition, HL was shown very weak two-photon excited fluorescence (TPEF). The tendency was also supported by the results of crystal structures and XPS determinations.

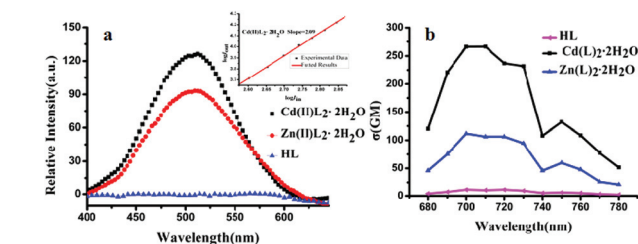


Fig. 7 (a) The two-photon fluorescence spectra of HL, $Cd(II)L_2(H_2O)_2$ and $Zn(II)L_2(H_2O)_2$ (1.0×10^{-3} M in ethyl acetate) at 720 nm. Inset: output fluorescence (I_{out}) vs. the square of input laser power (I_{in}^2) for $Cd(II)L_2(H_2O)_2$, $Zn(II)L_2(H_2O)_2$ and HL. Excitation carried out at 720 nm, with $c = 1.0 \times 10^{-3}$ mol L^{-1} in ethyl acetate. (b) Two-photon (from a 140 fs, 80 MHz, Ti:sapphire laser) absorption cross sections of HL, $Cd(II)L_2(H_2O)_2$, $Zn(II)L_2(H_2O)_2$ in THF *versus* excitation wavelengths of identical energy of 0.500 W.

Two-photon microscopy biological imaging application of $Zn(II)L_2(H_2O)_2$

As Zn has relatively low toxicity toward live cells, $Zn(II)L_2(H_2O)_2$ was selected for its bearing high quantum yield, large TPA

Table 2 The two-photon absorption cross-section σ_{tp} ($GM = 10^{-50}$ cm⁴ s per photon) of the six lowest excited states with the excitation energy E (eV) and the corresponding wavelength λ_{tp} (nm) in the gas phase

$Cd(II)L_2(H_2O)_2$			$Zn(II)L_2(H_2O)_2$			HL		
E	λ_{tp}	σ_{tp}	E	λ_{tp}	σ_{tp}	E	λ_{tp}	σ_{tp}
3.41	725.25	0.00	3.31	747.16	0.00	3.34	740.45	3.09
3.46	714.77	277.25	3.41	725.25	12.52	3.47	712.71	11.94
3.55	696.65	2.90	3.47	712.71	0.01	3.54	698.62	1.45
3.55	696.65	0.00	3.49	708.63	179.40	3.97	622.95	0.90
3.65	677.56	0.00	3.57	692.75	0.00	4.01	616.73	4.58
3.66	675.71	31.12	3.57	692.75	7.92	4.05	610.64	0.47

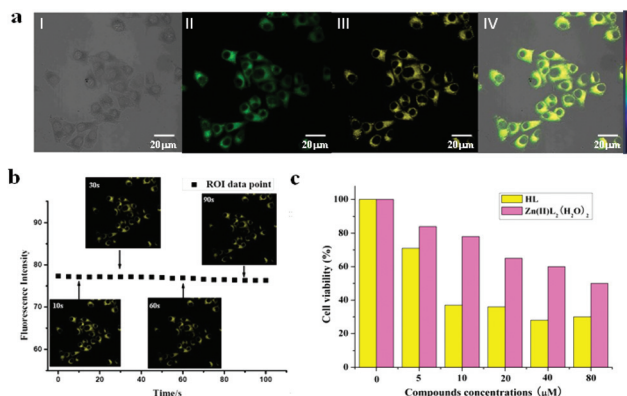


Fig. 8 (a) (I) Bright-field image of HepG2 cells. (II) One-photon image of HepG2 cells incubated with 20 μM Zn(II)L₂(H₂O)₂ after 20 min of incubation, washed by PBS buffer. $\lambda_{\text{ex}} = 330$ nm (emission wavelength from 440 to 499 nm). (III) Two-photon image of HepG2 cells incubated with 20 μM Zn(II)L₂(H₂O)₂ after 30 min of incubation, washed by PBS buffer. $\lambda_{\text{ex}} = 720$ nm (emission wavelength from 495 to 523 nm). (IV) The overlay of (a) to (c). Scale bars represent 20 μm. (b) Time series showing luminescence intensity of Zn(II)L₂(H₂O)₂ in a HepG2 cytosol region (20 μM, 20 min) under laser exposure over 100 s. Inset images from time point 0, 30, 60 and 90 s, scale bars represent 20 μm. (c) Cytotoxicity data results obtained from the MTT assay.

cross-section and long fluorescent lifetime. Fluorescent images of confocal microscopy and two-photon microscopy of HepG2 cells labeled with Zn(II)L₂(H₂O)₂ were captured. A bright-field image (Fig. 8a(I)) of each cell was taken immediately prior to the one-photon and two-photon microscopy (TPM) imaging. The green channel reveal HepG2 cells successfully uptake Zn(II)L₂(H₂O)₂, clearly, the luminescence located in cell cytosol (Fig. 8(b)(II) and (III)). The luminescence which comes from the cytosol supposes that the complex permeated the phospholipids bilayer of cellular membrane and bounded with cellular cytosol organelle. To further demonstrate the potential applications of Zn(II)L₂(H₂O)₂ for two photon microscopy (TPM) imaging in living cells, HepG2 cells were cultured and stained with Zn(II)L₂(H₂O)₂. The results showed that Zn(II)L₂(H₂O)₂ is clearly capable of detecting the cytoplasm section in HepG2 cells (Fig. 8(c)(IV)). Furthermore, Zn(II)L₂(H₂O)₂ (20 μM) in HepG2 cells cytosol region reveals higher stability upon laser irradiation during the period over 100 seconds (Fig. 8(b)), which reveals almost no photo-bleaching. The results showed that Zn(II)L₂(H₂O)₂ is cell-permeable and suitable for the cytosol staining, and exhibits the high fluorescent sensitivity relative to Zn(II)L₂(H₂O)₂ in live cells.

Considering their application in intracellular imaging, the MTT assay was performed to ascertain the cytotoxic effect of Zn(II)L₂(H₂O)₂ against HepG2 cells over a 24 h period. Cytotoxicity is a potential side effect of dyes that must be controlled when dealing with living cells or tissues. Fig. 8c shows the cell viability for HepG2 cells treated with Zn(II)L₂(H₂O)₂ at different concentrations for 24 h. The results clearly indicate that HepG2 cells incubated with concentration of 5 μM of Zn(II)-L₂(H₂O)₂ remain more than 80% viable after 24 h of feeding time, demonstrating the superior biocompatibility of Zn(II)-

L₂(H₂O)₂. Higher concentrations result in decreased cell survival, with 65% and 60% viability observed following 24 h of treatment with 20 and 40 μM Zn(II)L₂(H₂O)₂. As a result, cytotoxicity tests definitely indicate that the low-micromolar concentrations of Zn(II)L₂(H₂O)₂ have relatively low toxic effects on living cells over a period of 24 h, and Zn(II)L₂(H₂O)₂ indeed has great potentials for biological studies.

Conclusion

Two novel coordination compounds (Cd(II)L₂(H₂O)₂ Zn(II)-L₂(H₂O)₂) were synthesized and fully characterized. Both the results of time-dependent density functional theory (TD-DFT) and of the experimental studies indicated that the complexation of the β-diketone ligand lost a proton with metal ion extending the electronic delocalization in the coordination compounds, leading to dramatically enhanced two-photon absorption, especially, for the complex Cd(II)L₂(H₂O)₂. Therefore, it can be drawn that the coordination compounds for enhanced TPA properties may be a better strategy. In addition, Zn(II)L₂(H₂O)₂ shows potential as potential biological imaging probe for two-photon microscopy.

Acknowledgements

This work was supported by grants from the National Natural Science Foundation of China (21071001, 21271004, 51372003 and 21271003), the Natural Science Foundation of Anhui Province (1208085MB22, 1308085MB24), Ministry of Education Funded Projects Focus on returned overseas scholar, Program for New Century Excellent Talents in University (China) and Doctoral Program Foundation of Ministry of Education of China (20113401110004).

Notes and references

- 1 M. Göppert-Mayer, Fiber Elementarakte mit xwei QuantempWwgem Von Maria Göppert-Mayer, *Ann. Phys.*, 1931, **9**, 273.
- 2 W. Kaiser and C. G. Garret, *Phys. Rev. Lett.*, 1961, **7**, 229.
- 3 (a) B. H. Cumpston, S. P. Ananthavel, S. Barlow, D. L. Dyer, J. E. Ehrlich and L. L. Erskine, *Nature*, 1999, **398**, 51; (b) P. A. Bouit, G. Wetzels, G. Berginc, B. Loiseaux, L. Toupet and P. Feneyrou, *Chem. Mater.*, 2007, **19**, 5325; (c) S. Kawata, H. B. Sun, T. Tanaka and K. Takada, *Nature*, 2001, **412**, 697; (d) R. J. Xia, J. P. Malval, M. Jin, A. Spangenberg, D. C. Wan, H. T. Pu and T. Vergote, *Chem. Mater.*, 2012, **24**, 237; (e) H. M. Kim, C. Jung, B. R. Kim, S. Y. Jung, J. H. Hong and Y. G. Ko, *Angew. Chem., Int. Ed.*, 2007, **46**, 3460; (f) G. S. He, L. S. Tan, Q. D. Zheng and P. N. Prasad, *Chem. Res.*, 2008, **108**, 1245; (g) H. M. Kim and B. R. Cho, *Chem. Commun.*, 2009, 153; (h) L. Li, J. Y. Ge, H. Wu, Q. H. Xu and S. Q. Yao, *J. Am. Chem. Soc.*, 2012, **134**, 12157; (i) B. Kong, A. W. Zhu, C. Q. Ding,

- X. X. Zhao, B. Li and Y. Tian, *Adv. Mater.*, 2012, **24**, 5844;
- (j) H. Y. Ahn, K. E. Fairfull-Smith, B. J. Morrow, V. Lussini, B. Kim, M. V. Bondar, S. E. Bottle and K. D. Belfield, *J. Am. Chem. Soc.*, 2012, **134**, 4721.
- 4 (a) B. Wang, Y. C. Wang, J. L. Hua, Y. H. Jiang, J. H. Huang, S. X. Qian and H. Tian, *Chem.–Eur. J.*, 2011, **17**, 2647; (b) X. J. Li, X. H. Zhang, W. Li, Y. L. Wang, T. L. Liu, B. L. Zhang and W. J. Yang, *J. Mater. Chem.*, 2011, **21**, 3916; (c) Y. Hai, J. J. Chen, P. Zhao, H. B. Lv, Y. Yu, P. Y. Xu and J. L. Zhang, *Chem. Commun.*, 2011, **47**, 2435; (d) S. Sumalekshmy and J. F. Christoph, *Chem. Mater.*, 2011, **23**, 483; (e) M. G. Zhu, G. F. Zhang, C. Li and M. P. Aldred, *J. Am. Chem. Soc.*, 2011, **133**, 365; (f) N. Lin, W. X. Zhang, B. M. Koshel, J. X. Cheng and Y. Chen, *J. Phys. Chem.*, 2011, **115**, 3198; (g) A. L. Padilha, G. Nootz, P. D. Olszak, S. Webster and D. J. Hagan, *Nano Lett.*, 2011, **11**, 1227; (h) S. Yao and K. D. Belfield, *Eur. J. Org. Chem.*, 2012, 3199.
- 5 (a) Y. H. Jiang, Y. C. Wang, J. L. Hua, J. Tang, B. Li, S. X. Qian and H. Tian, *Chem. Commun.*, 2010, **46**, 4689; (b) Y. H. Jiang, Y. C. Wang, B. Wang, J. B. Yang, N. N. He, S. X. Qian and J. L. Hua, *Chem.–Eur. J.*, 2011, **17**, 2479.
- 6 (a) G. S. He, L.-S. Tan, Q. D. Zhang and P. N. Prasad, *Chem. Rev.*, 2008, **108**, 1245–1330; (b) M. Pawlicki, H. A. Collins, R. G. Denning and H. L. Anderson, *Angew. Chem., Int. Ed.*, 2009, **48**, 3244; (c) M. Albota, D. Beljonne, J.-L. Brédas, J. E. Ehrlich, J.-Y. Fu, A. A. Heikal, S. E. Hess, T. Kogej, M. D. Levin, S. R. Marder, D. McCord-Maughon, J. W. Perry, H. Röckel, M. Rumi, G. Subramaniam, W. W. Webb, X.-L. Wu and C. Xu, *Science*, 1998, **281**, 1653; (d) S. R. Marder, *Chem. Commun.*, 2006, 131.
- 7 (a) S. S. Zhou, X. Xue, J. F. Wang, Y. Dong, B. Jiang, D. Wei and M. L. Wan, *J. Mater. Chem.*, 2012, **22**, 22774; (b) B. J. Coe, J. Fielden, S. P. Foxon, B. S. Brunshwig and I. A. Selberghs, *J. Am. Chem. Soc.*, 2010, **132**, 3496; (c) C. Feuvrie, O. Maury, H. L. Bozec, I. Ledoux, J. P. Morrall, G. T. Dalton, M. Samoc and M. G. Humphrey, *J. Phys. Chem. A*, 2007, **111**, 8980; (d) M. P. Cifuentes, C. E. Powell, J. P. Morrall, A. M. McDonagh, N. T. Lucas and M. G. Humphrey, *J. Am. Chem. Soc.*, 2006, **128**, 10819; (e) C. K. Koo, K. L. Wong, W. Y. Man and Y. W. Lam, *Inorg. Chem.*, 2009, **48**, 872; (f) V. Chandrasekhar, R. Azhakar, B. Murugesapandian and T. Senapati, *Inorg. Chem.*, 2010, **49**, 4008; (g) C. K. M. Chan, C. H. Tao, H. L. Tam and N. Y. Zhu, *Inorg. Chem.*, 2009, **48**, 2855; (h) W. F. Sun, B. G. Zhang, Y. J. Li, T. M. Pritchett, Z. G. Li and J. E. Haley, *Chem. Mater.*, 2010, **22**, 6384; (i) Z. Q. Ji, Y. J. Li, M. P. Timothy, S. M. Nikolay and E. H. Joy, *Chem.–Eur. J.*, 2011, **17**, 2479.
- 8 (a) Y. H. Gao, J. Y. Wu, Y. M. Li, P. P. Sun, H. P. Zhou, J. X. Yang, S. Y. Zhang, B. K. Jin and Y. P. Tian, *J. Am. Chem. Soc.*, 2009, **131**, 5208; (b) D. M. Li, X. H. Tian, G. J. Hu, Q. Zhang, P. Wang and P. P. Sun, *Inorg. Chem.*, 2011, **50**, 7997; (c) X. C. Wang, X. H. Tian, Q. Zhang, P. P. Su, J. Y. Wu, H. P. Zhou and B. K. Jin, *Chem. Mater.*, 2012, **24**, 954; (d) Z. J. Hu, X. H. Tian, X. H. Zhao, P. Wang, Q. Zhang and P. P. Sun, *Chem. Commun.*, 2011, **47**, 12467; (e) Y. Ren, X.-Q. Yu, D.-J. Zhang, D. Wang, M.-L. Zhang, G.-B. Xu, X. Zhao, Y.-P. Tian, Z.-S. Shao and M.-H. Jiang, *J. Mater. Chem.*, 2002, **12**, 3431.
- 9 (a) N. Blouin and M. Leclerc, *Acc. Chem. Res.*, 2008, **41**, 1110; (b) W. S. Gevaerts, A. Furlan, M. M. Wienk and M. Turbiez, *Adv. Mater.*, 2012, **24**, 2130.
- 10 D. B. A. Raj, B. Francis, M. L. P. Reddy, R. R. Butorac, V. M. Lynch and A. H. Cowley, *Inorg. Chem.*, 2010, **49**, 9055.
- 11 J. N. Demas and G. A. Crosby, *J. Phys. Chem.*, 1971, **75**, 991.
- 12 T. G. Gray, C. M. Rudzinski, E. E. Meyer, R. H. Holm and D. G. Nocera, *J. Am. Chem. Soc.*, 2003, **125**, 4755.
- 13 C. Xu and W. W. Webb, *J. Opt. Soc. Am. B*, 1996, **13**, 481.
- 14 O. Varnavski, T. Goodson, L. Sukhomlinova and R. Twieg, *J. Phys. Chem. B*, 2004, **108**, 10484.
- 15 J. R. Lakowicz, *Principles of Fluorescence Spectroscopy*, Plenum Press, New York, 1983, p. 19.
- 16 J. H. Strickler and W. W. Webb, *Opt. Lett.*, 1991, **16**, 1780.
- 17 R. Cammi, M. Cossi and J. Tomasi, *J. Chem. Phys.*, 1996, **104**, 4611.
- 18 Y. R. Shen, *The Principles of Nonlinear Optics*, Wiley, New York, 1984.
- 19 (a) L. Yang, J. K. Feng and A. M. Ren, *J. Org. Chem.*, 2005, **70**, 5987; (b) GAUSSIAN 03, see <http://www.gaussian.com>
- 20 J. Olsen and P. Jorgensen, *J. Chem. Phys.*, 1985, **82**, 3235.
- 21 DALTON, Release Dalton, 2011, see <http://daltonprogram.org/cm>
- 22 P. He, H. H. Wang, S. G. Liu, J. X. Shi, G. Wang and M. L. Gong, *J. Phys. Chem. A*, 2009, **113**, 12885.
- 23 G. M. Sheldrick, *SADABS*, University of Göttingen, Göttingen, Germany, 1997.
- 24 L. J. Farrugia, *J. Appl. Crystallogr.*, 1999, **32**, 837.
- 25 G. M. Sheldrick, *SHELXL-97, Program for the Refinements of Crystal Structure*, University of Göttingen, Göttingen, Germany, 1997, p. 40.
- 26 B. M. Kariuki, K. D. M. Harris, D. Philp and J. M. A. Robinson, *J. Am. Chem. Soc.*, 1997, **119**, 12679.
- 27 Q. Zhang, W. L. Song, A. M. Showkot Hossain, Z. D. Liu, G. J. Hu, Y. P. Tian, J. Y. Wu, B. K. Jin, H. P. Zhou, J. X. Yang and S. Y. Zhang, *Dalton Trans.*, 2011, **40**, 3510.
- 28 Y. M. Berezin and S. L. Achilefu, *Chem. Res.*, 2010, **110**, 2641.
- 29 S. A. Patel, M. Cozzuol, J. M. Hales, C. I. Richards, M. Sartin, J. C. Hsiang, T. Vosch, J. W. Perry and R. M. Dickson, *J. Phys. Chem. C*, 2009, **113**, 20264.
- 30 S. M. Ji, J. Yang, Q. Yang, S. S. Liu, M. D. Chen and J. Z. Zhao, *J. Org. Chem.*, 2009, **74**, 4855.
- 31 M. Irie and K. Sayo, *J. Phys. Chem.*, 1992, **96**, 7671.